Identification of band structures and proposed one- and two-phonon γ-vibrational bands in ^{105}Mo

H. B. Ding,[1] S. J. Zhu,[1,2,*] J. H. Hamilton,[2] A. V. Ramayya,[2] J. K. Hwang,[2] K. Li,[2] Y. X. Luo,[2,3] J. O. Rasmussen,[3] I. Y. Lee,[3] C. T. Goodin,[2] X. L. Che,[1] Y. J. Chen,[1] and M. L. Li[1]

[1]*Department of Physics, Tsinghua University, Beijing 100084, People's Republic of China*

[2]*Department of Physics, Vanderbilt University, Nashville, Tennessee 37235, USA*

[3]*Lawrence Berkeley National Laboratory, Berkeley, California 94720, USA*

(Received 7 June 2006; revised manuscript received 27 August 2006; published 1 November 2006)

High-spin band structures in neutron-rich ^{105}Mo have been investigated by measuring prompt γ rays emitted by the spontaneous fission fragments of ^{252}Cf with the Gammasphere detector array. The yrast band has been confirmed and five new collective bands are observed. The three bands based on the 246.3-, 332.0-, and 310.0-keV levels are proposed as the single-neutron excitation bands built on the $3/2^+[411]$, $1/2^+[411]$, and $5/2^+[413]$ Nilsson orbitals, respectively. The other two bands with band head levels at 870.5 and 1534.6 keV are candidates for one-phonon $K = 9/2$ and two-phonon $K = 13/2$ γ-vibrational bands, respectively. Systematic comparison of these bands with bands in neighboring nuclei are discussed.

DOI: 10.1103/PhysRevC.74.054301 PACS number(s): 21.10.Re, 23.20.Lv, 27.60.+j, 25.85.Ca

I. INTRODUCTION

The neutron-rich Mo nuclei with $A > 100$ lie near the region of strongly deformed ground states. The reinforcement of proton and neutron shell gaps at the same large deformation, for $Z = 38$, 40 and $N = 60$, 62 [1] is the most widely accepted explanation for these strongly deformed ground states. The study of their high-spin states can provide important insight into the change in nuclear deformation and shape transition and single-particle and collective motions as one moves away from these shell gaps [1]. Studies [1–10] of the neutron-rich even-even $^{102-110}$Mo nuclei have revealed rich structural characteristics that include two quasiparticle bands in ^{104}Mo [5,6,8] and ^{106}Mo [4,7,8], one-phonon γ-vibrational bands in $^{102-108}$Mo [4–8], two-phonon γ-vibrational bands in ^{104,106}Mo [4–8], and possibly soft chiral vibrational bands in ^{106}Mo [10]. These results provide valuable information of the nuclear structures in this region. The investigation of collective bands in the odd-A Mo nuclei can allow one to compare the experiment results with calculations obtained from the Nilsson single-particle orbits. Previously, in neutron-rich odd-mass Mo isotopes, collective bands were investigated to higher spins in ^{103}Mo [2,8,11,12], ^{105}Mo [2,8,12], ^{107}Mo [2,13,14], and ^{109}Mo [13], including yrast bands as well as some side bands built on the single-neutron orbitals.

In the even-even isotopes in this region, the one-phonon γ-vibrational band was also observed in $^{108-112}$Ru [15–17] and $^{112-118}$Pd [18,19] in addition to those observed in $^{102-108}$Mo. For the odd-A nuclei, no extended one-phonon γ-vibrational band has been observed in these nuclei although band heads have been proposed in $Z = 45$ $^{105-111}$Rh [20–22], and an alternate interpretation of these second $11/2^+$ states being γ-band heads was presented for ^{105,107,109}Tc [23]. However, the experimental knowledge of two-phonon γ-bands is scarce. They have been observed only in a few nuclei, for example, in $Z = 67$ ^{168}Er [24] and ^{104,106}Mo [4–8]. So far, in the $A = 100$ neutron-rich region, no two-phonon γ-vibrational band structure was found in the odd-A nuclei. The ^{105}Mo nucleus is a good candidate to search for such a structure because its neutron number $N = 63$ lies between $N = 62$(^{104}Mo) and $N = 64$(^{106}Mo) where two-phonon γ bands are observed.

In this article, we report on observation of the collective bands in ^{105}Mo to high spins. Several new collective bands are established, and the one-phonon and two-phonon γ-vibrational bands are proposed. Prior to this work, in addition to higher-spin states in ^{105}Mo from spontaneous fission [2,12] and induced fission [8], the lower excitation levels have been studied through β decay [25,26] and the level systematics have been investigated in Ref. [27].

II. EXPERIMENTS AND RESULTS

The high-spin states of ^{105}Mo have been investigated by measuring the prompt γ rays emitted by the secondary fragments produced in the spontaneous fission of ^{252}Cf. The experiment was carried out at the Lawrence Berkeley National Laboratory. A ^{252}Cf source of strength $\sim$60 μCi was sandwiched between two Fe foils of thickness of 10 mg/cm^2 and was mounted in a 7.6-cm-diameter polyethylene ball to absorb β rays and conversion electrons. The source then was placed at the center of the Gammasphere detector array, which, for this experiment, consisted of 102 Compton-suppressed Ge detectors. A total of 5.7×10^{11} triple- and higher fold γ-coincidence events were collected. Thus, these data have higher statistics than our earlier measurements of Refs. [28–31] by a factor of about 15. The detailed information of the experiment can be found in other articles [22,23]. The coincidence data were analyzed with the Radware software package [32] using γ-γ-γ coincidence methods.

*Electronic address: zhushj@mail.tsinghua.edu.cn

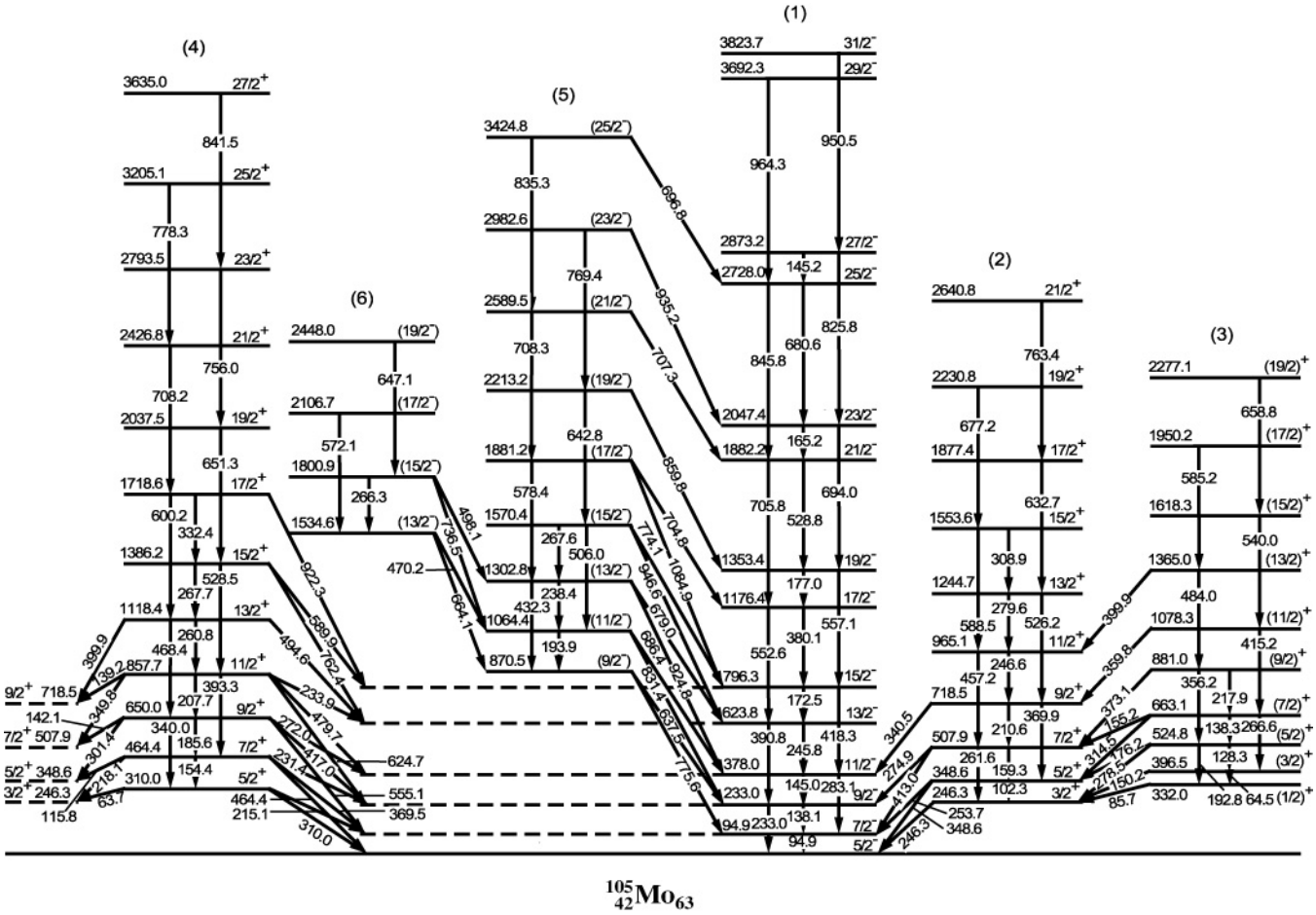

FIG. 1. Level scheme of ^{105}Mo obtained in the present work. Energies are in keV.

By carefully examining many coincidence relationships and transition intensities, a new high-spin level scheme of ^{105}Mo based on our new data is shown in Fig. 1. The collective bands observed are labeled at the top of Fig. 1. The results of our analysis such as the γ-transition energies, the relative intensities of transitions and the assignments of spin and parity (I^{π}) values are presented in Table I.

In the β-decay measurements from ^{105}Nb [25,26], the ground-state band of ^{105}Mo was identified up to 378.0 keV ($11/2^-$), and then it was extended up to 1353.4 keV ($19/2^-$) in earlier spontaneous fission measurements of ^{248}Cm [2] and up to 6075.3 keV ($39/2^-$) in the induced fission [8,12] studies. In this work, we identified the ground band levels up to 3823.7 keV ($31/2^-$). We did not observe the 4743.8- ($33/2^-$), 4893.9- ($35/2^-$) and 6075.3- ($39/2^-$) keV levels reported in Refs. [8,12]. But we added three new linking transitions of energies, 165.2 ($23/2^- \rightarrow 21/2^-$), 680.6 ($25/2^- \rightarrow 23/2^-$), and 145.2 ($27/2^- \rightarrow 25/2^-$) keV, inside this band. Five other new collective bands, labeled (2)–(6), with the band head levels at 246.3, 332.0, 310.0, 870.5, and 1534.6 keV, respectively, are established in the present work. Some low excitation levels have also been observed in Refs. [25,26], such as 247, 310, 332, 349, 397, 464, 508, and 525 keV, along with some transitions, in addition to those in the ground-state band. But these levels were not organized as members of any band except for the 247-, 349-, and 464-keV levels, which had been proposed as members of band (2) [26]. We confirmed the 246.3- and 348.6-keV levels as two members of band (2), but the 464.4-keV level belongs to another band labeled band (4). In Ref. [8], however, the 246.9-keV level is assigned as the band head with band members at 396.9, 662.3, 1077.7, 1616.5, and 2275.0 keV. In the present work, we confirmed the levels in that band with slightly different energies but replaced the 246.9 keV level with a new band head with energy of 332.0 keV and added four new $\Delta I = 1$ transitions in band (3). The 246.9 keV level belongs to a different band (2).

In spontaneous fission, a pair of correlated partners is produced. By gating on known γ rays in an isotope, one expects to see some transitions in its correlated partners. The partners of ^{105}Mo are ^{144}Ba ($3n$), ^{143}Ba ($4n$), and ^{142}Ba ($5n$). (Numbers in parentheses here indicate the number of neutrons emitted after fission.) As examples, we present several double-gating spectra for the data analysis. Figure 2(a) shows a spectrum from double gating on 94.9- [band (1) in ^{105}Mo] and 359.3- ($2^+ \rightarrow 0^+$ in ^{142}Ba) keV γ transitions. In this spectrum, in addition to observing the known transitions of the yrast band in ^{105}Mo and the partner nucleus ^{142}Ba, some new γ rays in ^{105}Mo, such as 159.3, 253.7, 369.5, 432.3, 506.0, 578.4, 664.1, and 775.6 keV, can be clearly seen. In Fig. 2(b), a spectrum from summing coincidence spectra

TABLE I. The γ-ray transition energies, the relative intensities, and the assignments of spin and parity (I^{π}) value for ^{105}Mo in this work.

E_γ (keV)	E_f (keV)	E_i (keV)	Assignment	Int. (%)	Mult.	Band
63.7	310.0	246.3	$5/2^+ \rightarrow 3/2^+$	2.0(4)	$M1$	$4 \rightarrow 2$
64.5	396.5	332.0	$(3/2^+) \rightarrow (1/2^+)$	0.8(1)	$(M1)$	3
85.7	332.0	246.3	$(1/2^+) \rightarrow 3/2^+$	3.7(4)	$(M1)$	$3 \rightarrow 2$
94.9	94.9	0.0	$7/2^- \rightarrow 5/2^-$	100(8)	$M1$	1
102.3	348.6	246.3	$5/2^+ \rightarrow 3/2^+$	13(1)	$M1$	2
115.8	464.4	348.6	$7/2^+ \rightarrow 5/2^+$	2.8(3)	$M1$	$4 \rightarrow 2$
128.3	524.8	396.5	$(5/2^+) \rightarrow (3/2^+)$	0.4(1)	$(M1)$	3
138.1	233.0	94.9	$9/2^- \rightarrow 7/2^-$	59(4)	$M1$	1
138.3	663.1	524.8	$(7/2^+) \rightarrow (5/2^+)$	0.3(1)	$(M1)$	3
139.2	857.7	718.5	$11/2^+ \rightarrow 9/2^+$	1.3(1)	$M1$	$4 \rightarrow 2$
142.1	650.0	507.9	$9/2^+ \rightarrow 7/2^+$	0.3(1)	$M1$	$4 \rightarrow 2$
145.0	378.0	233.0	$11/2^- \rightarrow 9/2^-$	37(3)	$M1$	1
145.2	2873.2	2728.0	$27/2^- \rightarrow 25/2^-$	<0.1	$M1$	1
150.2	396.5	246.3	$(3/2^+) \rightarrow 3/2^+$	5.5(6)	$(M1)$	$3 \rightarrow 2$
154.4	464.4	310.0	$7/2^+ \rightarrow 5/2^+$	2.4(3)	$M1$	4
155.2	663.1	507.9	$(7/2^+) \rightarrow 7/2^+$	1.3(2)	$(M1)$	$3 \rightarrow 2$
159.3	507.9	348.6	$7/2^+ \rightarrow 5/2^+$	7.1(8)	$M1$	2
165.2	2047.4	1882.2	$23/2^- \rightarrow 21/2^-$	0.7(1)	$M1$	1
172.5	796.3	623.8	$15/2^- \rightarrow 13/2^-$	9.4(1)	$M1$	1
176.2	524.8	348.6	$(5/2^+) \rightarrow 5/2^+$	2.8(3)	$(M1)$	$3 \rightarrow 2$
177.0	1353.4	1176.4	$19/2^- \rightarrow 17/2^-$	1.8(2)	$M1$	1
185.6	650.0	464.4	$9/2^+ \rightarrow 7/2^+$	5.7(5)	$M1$	4
192.8	524.8	332.0	$(5/2^+) \rightarrow (1/2^+)$	1.6(2)	$(E2)$	3
193.9	1064.4	870.5	$(11/2^-) \rightarrow (9/2^-)$	0.3(1)	$(M1)$	5
207.7	857.7	650.0	$11/2^+ \rightarrow 9/2^+$	2.0(2)	$M1$	4
210.6	718.5	507.9	$9/2^+ \rightarrow 7/2^+$	1.9(2)	$M1$	2
215.1	310.0	94.9	$5/2^+ \rightarrow 7/2^-$	0.9(2)	$E1$	$4 \rightarrow 1$
217.9	881.0	663.1	$(9/2^+) \rightarrow (7/2^+)$	<0.1	$(M1)$	3
218.1	464.4	246.3	$7/2^+ \rightarrow 3/2^+$	0.6(1)	$E2$	$4 \rightarrow 2$
231.4	464.4	233.0	$7/2^+ \rightarrow 9/2^-$	0.7(1)	$E1$	$4 \rightarrow 1$
233.0	233.0	0.0	$9/2^- \rightarrow 5/2^-$	20(2)	$E2$	1
233.9	857.7	623.8	$11/2^+ \rightarrow 13/2^-$	0.7(1)	$E1$	$4 \rightarrow 1$
238.4	1302.8	1064.4	$(13/2^-) \rightarrow (11/2^-)$	0.8(1)	$(M1)$	5
245.8	623.8	378.0	$13/2^- \rightarrow 11/2^-$	18(2)	$M1$	1
246.3	246.3	0.0	$3/2^+ \rightarrow 5/2^-$	35(3)	$E1$	$2 \rightarrow 1$
246.6	965.1	718.5	$11/2^+ \rightarrow 9/2^+$	0.7(2)	$M1$	2
253.7	348.6	94.9	$5/2^+ \rightarrow 7/2^-$	8.1(9)	$E1$	$2 \rightarrow 1$
260.8	1118.4	857.7	$13/2^+ \rightarrow 11/2^+$	1.5(2)	$M1$	4
261.6	507.9	246.3	$7/2^+ \rightarrow 3/2^+$	1.8(3)	$E2$	2
266.3	1800.9	1534.6	$(15/2^-) \rightarrow (13/2^-)$	0.3(1)	$(M1)$	6
266.6	663.1	396.5	$(7/2^+) \rightarrow (3/2^+)$	3.4(3)	$(E2)$	3
267.6	1570.4	1302.8	$(15/2^-) \rightarrow (13/2^-)$	0.8(2)	$(M1)$	5
267.7	1386.2	1118.4	$15/2^+ \rightarrow 13/2^+$	0.3(1)	$M1$	4
272.0	650.0	378.0	$9/2^+ \rightarrow 11/2^-$	0.7(1)	$E1$	$4 \rightarrow 1$
274.9	507.9	233.0	$7/2^+ \rightarrow 9/2^-$	2.2(3)	$E1$	$2 \rightarrow 1$
278.5	524.8	246.3	$(5/2^+) \rightarrow 3/2^+$	4.9(5)	$(M1)$	$3 \rightarrow 2$
279.6	1244.7	965.1	$13/2^+ \rightarrow 11/2^+$	0.4(1)	$M1$	2
283.1	378.0	94.9	$11/2^- \rightarrow 7/2^-$	30(3)	$E2$	1
301.4	650.0	348.6	$9/2^+ \rightarrow 5/2^+$	2.5(2)	$E2$	$4 \rightarrow 2$
308.1	1176.4	796.3	$17/2^- \rightarrow 15/2^-$	4.4(5)	$M1$	1
308.9	1553.6	1244.7	$15/2^+ \rightarrow 13/2^+$	<0.1	$M1$	2
310.0	310.0	0.0	$5/2^+ \rightarrow 5/2^-$	12(2)	$E1$	$4 \rightarrow 1$
314.5	663.1	348.6	$(7/2^+) \rightarrow 5/2^-$	1.4(2)	$(M1)$	$3 \rightarrow 2$
332.4	1718.6	1386.2	$17/2^+ \rightarrow 15/2^+$	0.2(1)	$M1$	4
340.0	650.0	310.0	$9/2^+ \rightarrow 5/2^+$	3.4(4)	$E2$	4
340.5	718.5	378.0	$9/2^+ \rightarrow 11/2^-$	0.3(1)	$E1$	$2 \rightarrow 1$
348.6	348.6	0.0	$5/2^+ \rightarrow 5/2^-$	8.7(9)	$E1$	$2 \rightarrow 1$
349.8	857.7	507.9	$11/2^+ \rightarrow 7/2^+$	0.5(1)	$E2$	$4 \rightarrow 2$
356.2	881.0	524.8	$(9/2^+) \rightarrow (5/2^+)$	1.7(2)	$(E2)$	3
359.8	1078.3	718.5	$(11/2^+) \rightarrow 9/2^+$	0.2(1)	$(M1)$	$3 \rightarrow 2$
369.5	464.4	94.9	$7/2^+ \rightarrow 7/2^-$	4.4(6)	$E1$	$4 \rightarrow 1$
369.9	718.5	348.6	$9/2^+ \rightarrow 5/2^+$	3.1(3)	$E2$	2
373.1	881.0	507.9	$(9/2^+) \rightarrow 7/2^+$	0.3(1)	$(M1)$	$3 \rightarrow 2$
380.1	1176.4	796.3	$17/2^- \rightarrow 15/2^-$	4.4(5)	$M1$	1
390.8	623.8	233.0	$13/2^- \rightarrow 9/2^-$	21(2)	$E2$	1
393.3	857.7	464.4	$11/2^+ \rightarrow 7/2^+$	5.3(5)	$E2$	4
399.9	1365.0	965.1	$(31/2^+) \rightarrow 11/2^+$	0.3(1)	$(M1)$	$3 \rightarrow 2$
399.9	1118.4	718.5	$13/2^+ \rightarrow 9/2^+$	0.2(1)	$E2$	$4 \rightarrow 2$
413.0	507.9	94.9	$7/2^+ \rightarrow 7/2^-$	0.9(2)	$E1$	$2 \rightarrow 1$
415.2	1078.3	663.1	$(11/2^+) \rightarrow (7/2^+)$	1.8(2)	$(E2)$	3
417.0	650.0	233.0	$9/2^+ \rightarrow 9/2^-$	3.7(2)	$E1$	$4 \rightarrow 1$
418.3	796.3	378.0	$15/2^- \rightarrow 11/2^-$	34(2)	$E2$	1
432.3	1302.8	870.5	$(13/2^-) \rightarrow (9/2^-)$	3.0(4)	$(E2)$	5
457.2	965.1	507.9	$11/2^+ \rightarrow 7/2^+$	2.4(3)	$E2$	2
464.4	464.4	0.0	$7/2^+ \rightarrow 5/2^-$	1.7(3)	$E1$	$4 \rightarrow 1$
468.4	1118.4	650.0	$13/2^+ \rightarrow 9/2^+$	5.5(6)	$E2$	4
470.2	1534.6	1064.4	$(13/2^-) \rightarrow (11/2^-)$	0.5(1)	$(M1)$	$6 \rightarrow 5$
479.7	857.7	378.0	$11/2^+ \rightarrow 11/2^-$	1.9(3)	$E1$	$4 \rightarrow 1$
484.0	1365.0	881.0	$(13/2^+) \rightarrow (9/2^+)$	0.7(1)	$(E2)$	3
494.6	1118.4	623.8	$13/2^+ \rightarrow 13/2^-$	1.7(2)	$E1$	$4 \rightarrow 1$
498.1	1800.9	1302.8	$(15/2^-) \rightarrow (13/2^-)$	0.5(2)	$(M1)$	$6 \rightarrow 5$
506.0	1570.4	1064.4	$(15/2^-) \rightarrow (11/2^-)$	2.9(6)	$(E2)$	5
526.2	1244.7	718.5	$13/2^+ \rightarrow 9/2^+$	2.9(3)	$E2$	2
528.5	1386.2	857.7	$15/2^+ \rightarrow 11/2^+$	2.7(4)	$E2$	4
528.8	1882.2	1353.4	$21/2^- \rightarrow 19/2^-$	1.1(2)	$M1$	1
540.0	1618.3	1078.3	$(15/2^+) \rightarrow (11/2^+)$	0.9(1)	$(E2)$	3
552.6	1176.4	623.8	$17/2^- \rightarrow 13/2^-$	12(1)	$E2$	1
555.1	650.0	94.9	$9/2^+ \rightarrow 7/2^-$	1.8(1)	$E1$	$4 \rightarrow 1$
557.1	1353.4	796.3	$19/2^- \rightarrow 15/2^-$	22(2)	$E2$	1
572.1	2106.7	1534.6	$(17/2^-) \rightarrow (13/2^-)$	1.0(1)	$(E2)$	6
578.4	1881.2	1302.8	$(17/2^-) \rightarrow (13/2^-)$	1.9(3)	$(E2)$	5
585.2	1950.2	1365.0	$(17/2^+) \rightarrow (13/2^+)$	0.3(1)	$(E2)$	3
588.5	1553.6	965.1	$15/2^+ \rightarrow 11/2^+$	0.7(1)	$E2$	2
589.9	1386.2	796.3	$15/2^+ \rightarrow 15/2^-$	1.8(3)	$E1$	$4 \rightarrow 1$
600.2	1718.6	1118.4	$17/2^+ \rightarrow 13/2^+$	3.6(4)	$E2$	4
624.7	857.7	233.0	$11/2^+ \rightarrow 9/2^-$	2.7(3)	$E1$	$4 \rightarrow 1$
632.7	1877.4	1244.7	$17/2^+ \rightarrow 13/2^+$	1.7(4)	$E2$	2
637.5	870.5	233.0	$(9/2^-) \rightarrow 9/2^-$	3.7(5)	$(M1)$	$5 \rightarrow 1$
642.8	2213.2	1570.4	$(19/2^-) \rightarrow (15/2^-)$	1.8(3)	$(E2)$	5
647.1	2448.0	1800.9	$(19/2^-) \rightarrow (15/2^-)$	0.6(1)	$(E2)$	6
651.3	2037.5	1386.2	$19/2^+ \rightarrow 15/2^+$	1.5(2)	$E2$	4
658.8	2277.1	1618.3	$(19/2^+) \rightarrow (15/2^+)$	0.4(1)	$(E2)$	3
664.1	1534.6	870.5	$(13/2^-) \rightarrow (9/2^-)$	2.3(3)	$(E2)$	$6 \rightarrow 5$
677.2	2230.8	1553.6	$19/2^+ \rightarrow 15/2^+$	0.3(1)	$E2$	2
679.0	1302.8	623.8	$(13/2^-) \rightarrow 13/2^-$	2.5(3)	$(M1)$	$5 \rightarrow 1$
680.6	2728.0	2047.4	$25/2^- \rightarrow 23/2^-$	0.4(2)	$M1$	1
686.4	1064.4	378.0	$(11/2^-) \rightarrow 11/2^-$	4.1(4)	$(M1)$	$5 \rightarrow 1$
694.0	2047.4	1353.4	$23/2^- \rightarrow 19/2^-$	13(1)	$E2$	1
696.8	3424.8	2728.0	$(25/2^-) \rightarrow 25/2^-$	<0.1	$(M1)$	$5 \rightarrow 1$
704.8	1881.2	1176.4	$(17/2^-) \rightarrow 17/2^-$	1.7(3)	$(M1)$	$5 \rightarrow 1$

TABLE I. *(Continued.)*

E_γ (keV)	E_f (keV)	E_i (keV)	Assignment	Int. (%)	Mult.	Band
705.8	1882.2	1176.4	$21/2^- \rightarrow 17/2^-$	8.7(8)	$E2$	1
707.3	2589.5	1882.2	$(21/2^-) \rightarrow 21/2^-$	0.5(2)	$(M1)$	$5 \rightarrow 1$
708.2	2426.8	1718.6	$21/2^+ \rightarrow 17/2^+$	1.9(3)	$E2$	4
708.3	2589.5	1881.2	$(21/2^-) \rightarrow (17/2^-)$	1.1(3)	$(E2)$	5
736.5	1800.9	1064.4	$(15/2^-) \rightarrow (11/2^-)$	1.1(1)	$(E2)$	$6 \rightarrow 5$
756.0	2793.5	2037.5	$23/2^+ \rightarrow 19/2^+$	0.4(1)	$E2$	4
762.4	1386.2	623.8	$15/2^+ \rightarrow 13/2^-$	<0.1	$E1$	$4 \rightarrow 1$
763.4	2640.8	1877.4	$21/2^+ \rightarrow 17/2^+$	0.8(1)	$E2$	2
769.4	2982.6	2213.2	$(23/2^-) \rightarrow (19/2^-)$	0.7(1)	$(E2)$	5
774.1	1570.4	796.3	$(15/2^-) \rightarrow 15/2^-$	1.3(4)	$(M1)$	$5 \rightarrow 1$
775.6	870.5	94.9	$(9/2^-) \rightarrow 7/2^-$	7.6(1)	$(M1)$	$5 \rightarrow 1$
778.3	3205.1	2426.8	$25/2^+ \rightarrow 21/2^+$	0.6(1)	$E2$	4
825.8	2873.2	2047.4	$27/2^- \rightarrow 23/2^-$	1.8(2)	$E2$	1
831.4	1064.4	233.0	$(11/2^-) \rightarrow 9/2^-$	5.3(9)	$(M1)$	$5 \rightarrow 1$
835.3	3424.8	2589.5	$(25/2^-) \rightarrow (21/2^-)$	0.6(1)	$(E2)$	5
841.5	3635.0	2793.5	$27/2^+ \rightarrow 23/2^+$	<0.1	$E2$	4
845.8	2728.0	1882.2	$25/2^- \rightarrow 21/2^-$	4.4(5)	$E2$	1
859.8	2213.2	1353.4	$(19/2^-) \rightarrow 19/2^-$	1.4(2)	$(M1)$	$5 \rightarrow 1$
922.3	1718.6	796.3	$17/2^+ \rightarrow 15/2^-$	0.7(1)	$E1$	$4 \rightarrow 1$
924.8	1204.8	378.0	$(13/2^-) \rightarrow 11/2^-$	2.6(3)	$(M1)$	$5 \rightarrow 1$
935.2	2982.6	2047.4	$(23/2^-) \rightarrow 23/2^-$	0.4(1)	$(M1)$	$5 \rightarrow 1$
946.6	1570.4	623.8	$(15/2^-) \rightarrow 13/2^-$	0.7(1)	$(M1)$	$5 \rightarrow 1$
950.5	3823.7	2873.2	$31/2^- \rightarrow 27/2^-$	0.4(1)	$E2$	1
964.3	3692.3	2728.0	$29/2^- \rightarrow 25/2^-$	1.8(3)	$E2$	1
1084.9	1881.2	796.3	$(17/2^-) \rightarrow 15/2^-$	1.2(2)	$(M1)$	$5 \rightarrow 1$

with double gating on the 310.0- and 340.0-keV, and 393.3- and 651.3-keV γ transitions is given. From this spectrum, the transitions in band (4) and some linking ones between bands (4) and (1) can be seen, such as 218.1-, 369.5-, 468.4-, 528.5-, 600.2-, and 708.2 keV transitions. In Figs. 3(a) and 3(b), the two coincidence spectra are generated by double gating on 246.3- and 102.3-keV and 246.3- and 150.2-keV γ transitions, respectively. One can clearly see the γ transitions in bands (2) and (3), such as the 159.3-, 210.6-, 246.6-, 369.9-, 526.2- and 632.7 keV transitions of band (2) in spectrum (a) and the 128.3-, 138.3-, 266.6-, 415.2-, 540.0-, and 658.8-keV transitions of band (3) in spectrum (b). Figure 4 shows the partial coincidence spectrum obtained by double gating on the 94.9- and 775.6-keV γ transitions. In this spectrum, the main γ transitions in bands (5) and (6), such as the 432.3-, 506.0-, 572.1-, 578.4-, 647.1-, 664.1-, 708.3-, and 835.3-keV transitions, are clearly seen. In Figs. 2(b), 3, and 4, in addition to the γ peaks observed in ^{105}Mo, the main γ transitions in the partner nuclei $^{142-144}$Ba can also be seen.

III. DISCUSSION

It has been shown that the $N = 63$ ^{101}Sr, ^{103}Zr, and ^{105}Mo isotones have large β_2 deformations [26,27]. In the neighboring $Z = 44$, ^{108,110,112}Ru isotopes, large triaxiality has been suggested [1,15–17]. To understand the structural properties observed in ^{105}Mo, we have carried out the total Routhian surfaces (TRS) calculations using the cranked shell model (CSM), described in detail by Bengtsson and Frauendorf *et al.* [33–35]. The calculated results of TRS for ^{105}Mo are presented in Fig. 5, from which the minima can be found at $\beta_2 = 0.309$, $\beta_4 = 0.014$, and $\gamma = -18.9^\circ$ for $\omega = 0.0$ MeV/$\hbar$ and $\beta_2 = 0.321$, $\beta_4 = 0.012$, and $\gamma = -19.2^\circ$ for $\omega = 0.3$ MeV/$\hbar$. The β_2 value slightly changes with increasing rotational frequency ω, but the γ value is stable. The calculated results indicate that the ^{105}Mo nucleus has triaxiality, but the γ-value is less than that in the Ru isotopes.

According to the deformed shell model, the observed collective bands in ^{105}Mo should originate from single-neutron configurations. To search for the band assignments, we also carried out the single-particle energy calculations using the Nilsson model. The calculated Nilsson diagram for neutrons in ^{105}Mo is presented in Fig. 6. For the $N = 63$ ^{105}Mo with the β_2 parameter between 0.3 and 0.4, the single-neutron orbitals expected near the Fermi level are $3/2^+[411]$, $5/2^+[413]$, $5/2^-[532]$, $1/2^+[411]$, $7/2^-[523]$, and $5/2^+[402]$. These orbitals will help us to assign the configurations of the collective bands observed in ^{105}Mo.

A. Band (1)

The yrast band (1) has been assigned as $K^\pi = 5/2^-$ based on the $5/2^-[532]$ orbital of the $\nu h_{11/2}$ subshell [2,8,12,26,27]. The $\nu h_{11/2}$ negative-parity band structure has also been identified in $N = 63$ isotones ^{103}Zr [8] and ^{107}Ru [36], as well as in ^{103}Mo [8,11] and ^{107}Mo [14]. These bands show decoupled characteristics. They have large signature splitting between $\alpha = +1/2$ and $\alpha = -1/2$ components. The plots of the level energy difference of the $\nu h_{11/2}$ bands as a function of the spin I in the $Z = 42$ isotopes ^{103,105,107}Mo, and in the $N = 63$ isotones ^{103}Zr, ^{105}Mo, and ^{107}Ru are shown in Fig. 7. One can see that among the Mo isotopes, ^{103}Mo shows a larger signature splitting especially at the lower spins, whereas ^{105,107}Mo have almost identical splittings. However, in ^{103}Zr, ^{105}Mo, and ^{107}Ru, the splitting increases with increasing Z number. Particle-triaxial rotor model calculations [8] indicate that the trend of signature splitting of the $\nu h_{11/2}$ orbitals in odd-A nuclei is very sensitive to the γ degree of freedom. This means that the signature splitting increases with an increasing γ value. The γ values are $\sim 0^\circ$ in Zr, $\sim -19^\circ$ in Mo, and ~ -22 to -29° in Ru [1,15,16]. So ^{105}Mo has a medium γ degree of freedom. It is interesting that the splitting is largest for ^{103}Mo with the smallest neutron number compared to ^{105,107}Mo and is even larger than the splitting for ^{107}Ru. This same trend with N was found in the neighboring odd-A ^{101,103,105}Nb ground bands where γ values of -19°, -15°, and -13° were found, respectively [37]. However, in ^{105,107,109,111}Tc, the signature splitings increase slowly with the increasing N with $\gamma = -22.5^\circ$, -25°, and -26°, giving the best fitting with the data for ^{107,109,111}Tc, respectively [38]. Thus there is an interesting open question concerning the reversal in trends of γ with increasing neutron number.

B. Bands (2), (3), and (4)

Observed bands (2), (3), and (4) in ^{105}Mo have similar level patterns with more regular level spacings than those in band (1) and show the characteristics of a normal rotational band of

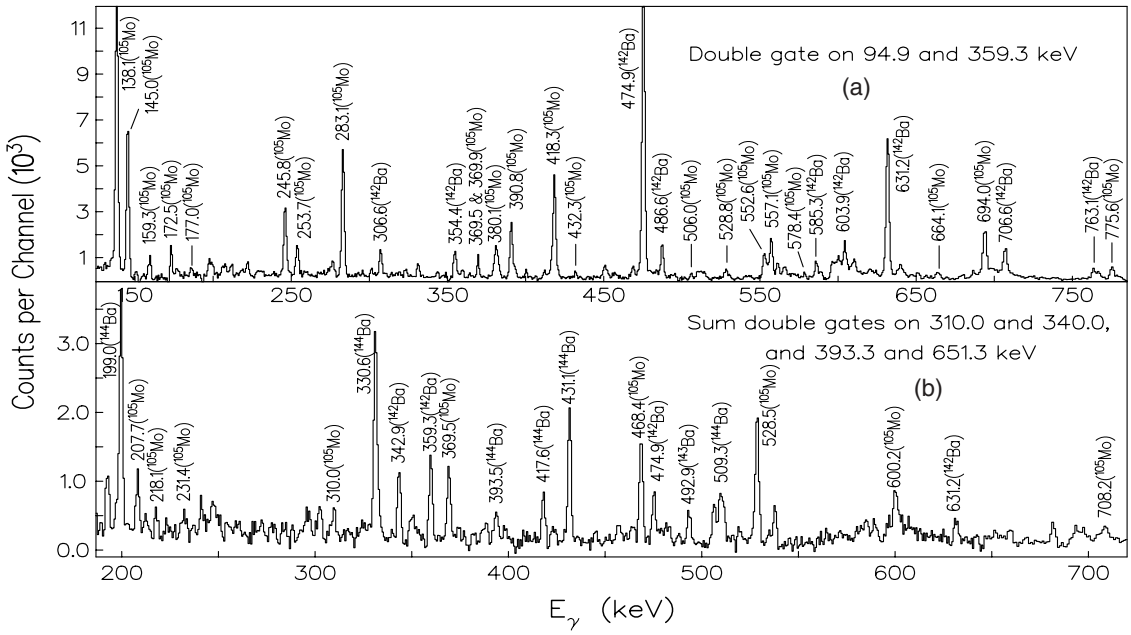

FIG. 2. Portion of selected γ-ray spectra obtained from triple coincidences by (a) double gating on the 94.9-keV transition in ^{105}Mo and the 359.3-keV transition in ^{142}Ba, and (b) summed coincidence spectra obtained by double gating on transitions of 310.0 and 340.0 keV, and 393.3 and 651.3 keV in band (4) of ^{105}Mo.

odd-A nuclei built on a single-particle configuration. So their origin should differ from that of band (1). Based on the early reports and systematic comparison with neighboring nuclei, we assign positive parity to these bands. In the early β-decay measurements [26,27], the I^{π}s of the levels at 246.3 and 310.0 keV, now the band head levels of bands (2) and (4), were assigned as $3/2^+$ and $5/2^+$, associated with the $3/2^+[411]$ and $5/2^+[413]$ Nilsson orbitals, respectively. So we assume that bands (2) and (4) have $K^{\pi} = 3/2^+$ and $5/2^+$, respectively. The $3/2^+[411]$ band was also observed in the neighboring isotopes ^{103}Mo [11,12] and ^{107}Mo [14]. The $5/2^+[413]$ band was observed in ^{107}Mo [14]. The band head at 332.0 keV observed in Ref. [27] was tentatively assigned as $1/2^+$ based on the $1/2^+$ [411] Nilsson orbital. But this $1/2^+$ band has not been observed in the neighboring Mo isotopes. Based on the regular spacings and the γ-transition intensities,

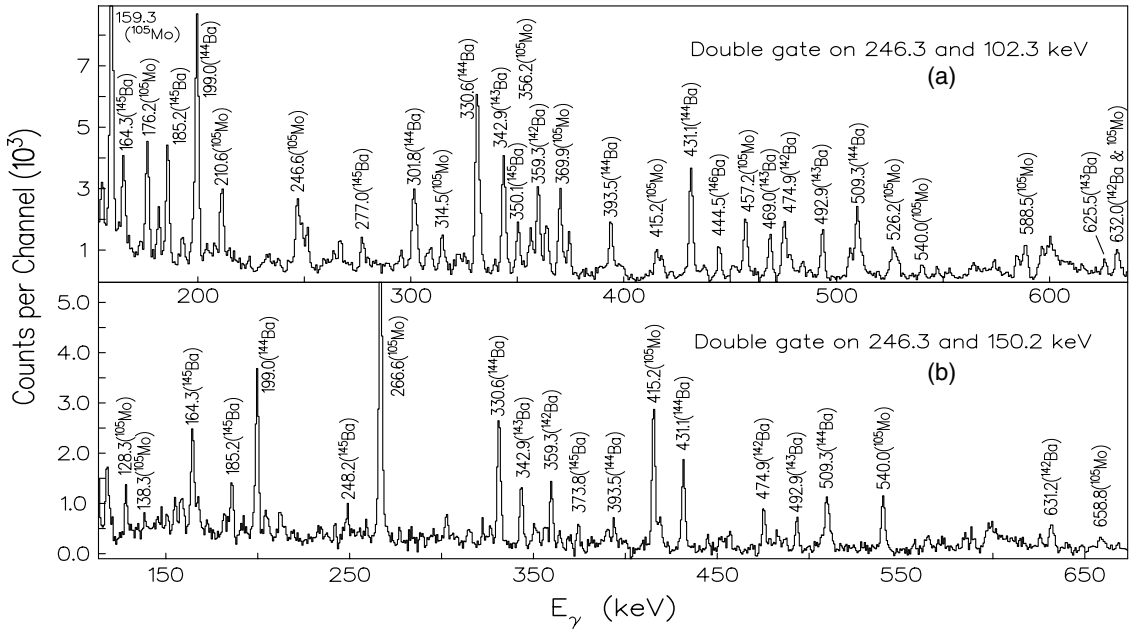

FIG. 3. Coincidence γ-ray spectra obtained by double gating on the (a) 246.3- and 102.3-keV transitions and (b) 246.3- and 150.2-keV transitions in ^{105}Mo.

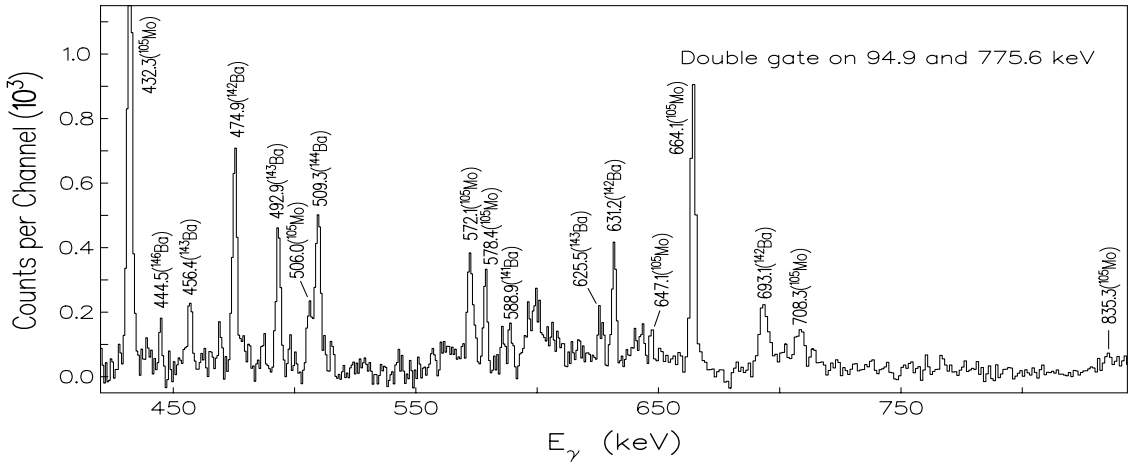

FIG. 4. Portion of coincidence γ-ray spectrum obtained by double gating on 94.9- and 775.6-keV transitions in ^{105}Mo.

we assign the I^πs of the other levels in each band observed in ^{105}Mo, as shown in Fig. 1. Bands (2)–(4) consist of the two signature partner bands with $\Delta I = 2$ transitions along with some $\Delta I = 1\,M1$ linking transitions between them. These assignments for the positive-parity bands for ^{105}Mo are consistent with the Nilsson diagram for neutrons as shown in Fig. 6.

To carry out further systematic comparisons, we have calculated the total angular momentum alignment I_x as a function of the rotational frequency ω by using the formula $I_x = \sqrt{(I_a + 1/2)^2 - K^2}$, where $I_a = (I_i + I_f)/2$, $\hbar\omega = (E_i - E_f)/2$. We assumed $K = 3/2$, 1/2, and 5/2 for the $3/2^+[411]$, $1/2^+[411]$, and $5/2^+[413]$ bands, respectively. The results for ^{105,107}Mo along with the neighboring even-even nuclei ^{104,106}Mo are shown in Fig. 8. The single-particle alignment i in each band can be estimated from the difference between I_x values for the band of the odd-A Mo nucleus and the $K = 0$ ground-state band of the neighboring even-even Mo nuclei. For the $3/2^+[411]$ band, the single-particle alignment has an average values of $i \sim 0.2\ \hbar$ in ^{105}Mo and $\sim 0.8\ \hbar$ in ^{107}Mo, respectively. For the $5/2^+[413]$ band, the average values of i are $\sim 0.6\hbar$ in the ^{105}Mo and ^{106}Mo. One can see that the single-particle alignments i are close to each other in the positive-parity bands of ^{105}Mo and ^{107}Mo. These results give further confidence for assigning the configurations for bands (2) and (3). For the $1/2^+[411]$ band, the average alignment value of $i \sim 0.9\ \hbar$ is obtained.

Figure 9 shows the plot of moments of inertia J_1 versus the rotation frequency $\hbar\omega$ for the even-parity bands in ^{105}Mo along with those in ^{103,107}Mo. One can see that the smoothly increasing trends of J_1 with $\hbar\omega$ are very similar. They vary between 20 and 32 $\hbar^2$/MeV.

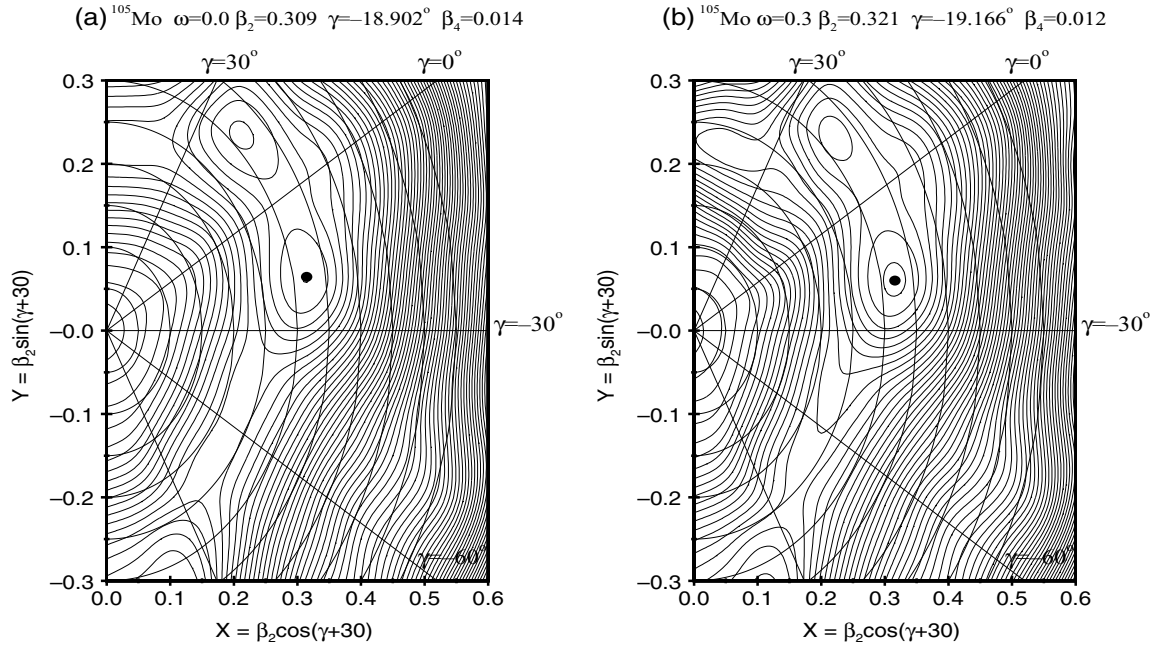

FIG. 5. Polar coordinate plots of the total Routhian surface (TRS) calculated at (a) $\omega = 0.0$ MeV/$\hbar$ and (b) $\omega = 0.3$ MeV/$\hbar$ for ^{105}Mo.

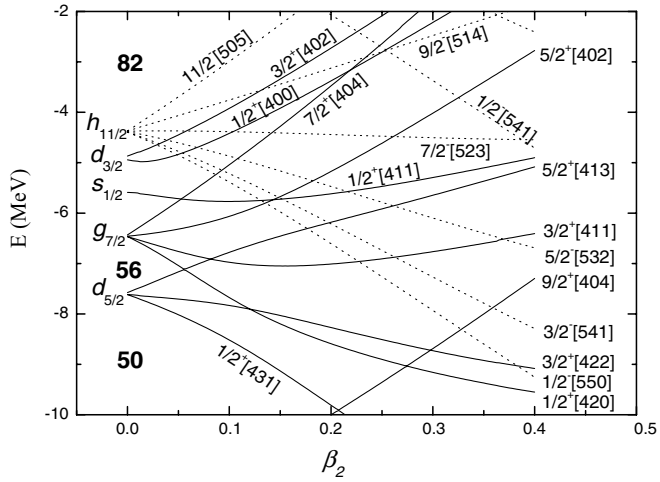

FIG. 6. Partial Nilsson diagram for neutrons of $^{105}_{42}Mo_{63}$.

C. Bands (5) and (6)

New bands (5) and (6) are established in the present work. Based on the observed pattern of decay transitions from band (5) to band (1), the possible spin of the band-head level of band (5) could be 9/2 or 11/2. The excitation energy at 870.5 keV of the band head indicates that this level originates from a single-neutron orbital or belongs to a one-phonon γ-vibrational state. If it belongs to a single-neutron excitation, we can exclude the $9/2^+$ or $11/2^+$ states because there is not a suitable orbital in a Nilsson diagram around the Fermi surface, as seen in Fig. 6. For a negative-parity state, the possible choice is $9/2^-[514]$ or $11/2^-[505]$ orbital excitation. But these two orbitals would seem to be still too far from the Fermi surface to be possible. So band (5) most probably is an one phonon γ-vibrational band with $K = 9/2$ built on the $5/2^-$ ground state and the state at the 870.5-keV level is then $9/2^-$. The absence of a $9/2^- \rightarrow 5/2^-$, 870-keV ground state transition may be a result of the triaxial nature of ^{105}Mo giving rise to different branching ratios compared to those for a symmetric rotor. Such differences we found for the second $11/2^+$ state in ^{105,107,109}Tc [23] and ^{111,113}Rh [22] which decay strongly to the $9/2^+$ ground band members but only very very weakly to the $7/2^+$ ground states. Band (6) has a band-head excitation energy at 1534.6 keV based on the observed transitions to

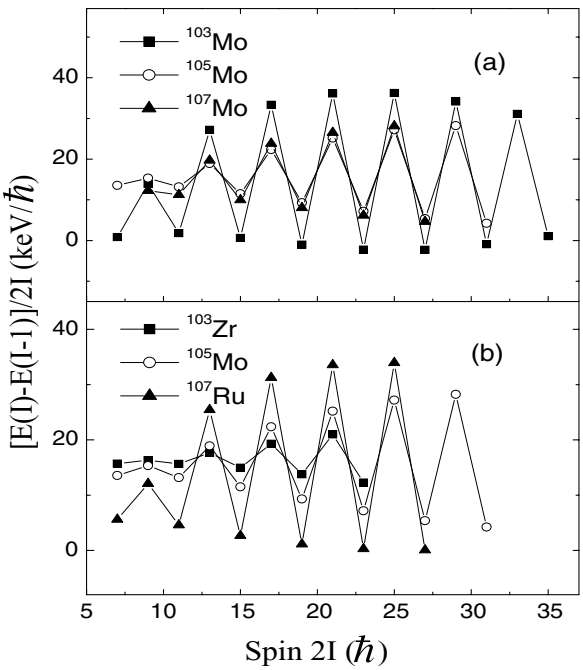

FIG. 7. Signature splitting for the $\nu h_{11/2}$ bands as a function of the spin I (a) in ^{103}Mo [8,11], ^{105}Mo (present work), and ^{107}Mo [14] and (b) in ^{103}Zr [8], ^{105}Mo (present work), and ^{107}Ru [36].

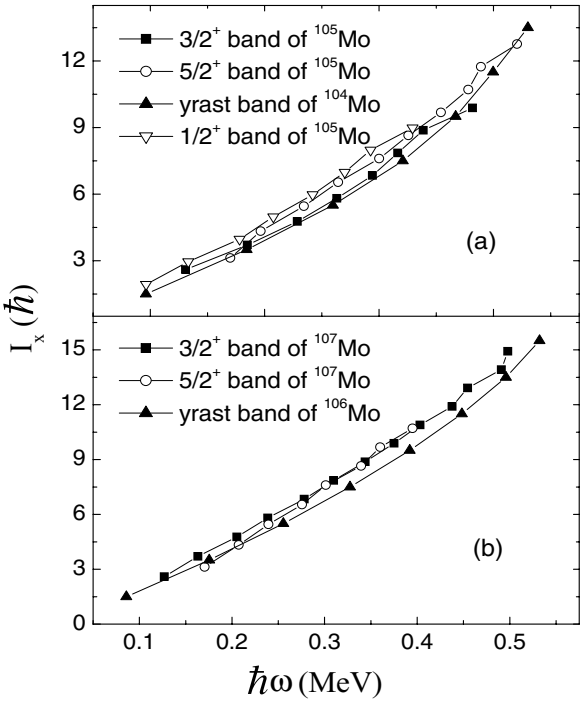

FIG. 8. Total angular momentum alignment I_x in $1/2^+[411]$, $3/2^+[411]$, and $5/2^+[413]$ bands of ^{105}Mo, and $3/2^+[411]$, $5/2^+[413]$ bands of ^{107}Mo.

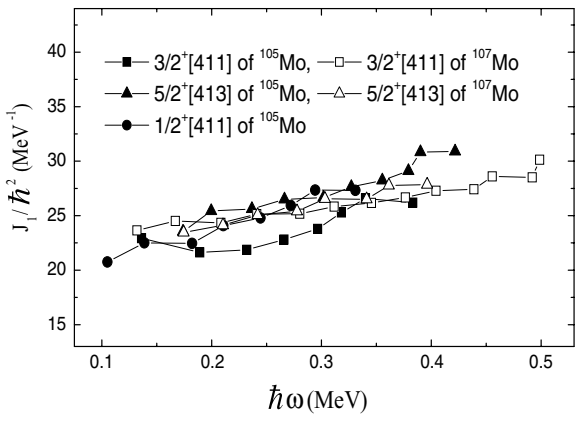

FIG. 9. Plot of moment of inertia J_1 vs. frequency $\hbar\omega$ for $1/2^+[411]$, $3/2^+[411]$, and $5/2^+[413]$ bands of ^{105}Mo, and $3/2^+[411]$, $5/2^+[413]$ bands of ^{107}Mo.

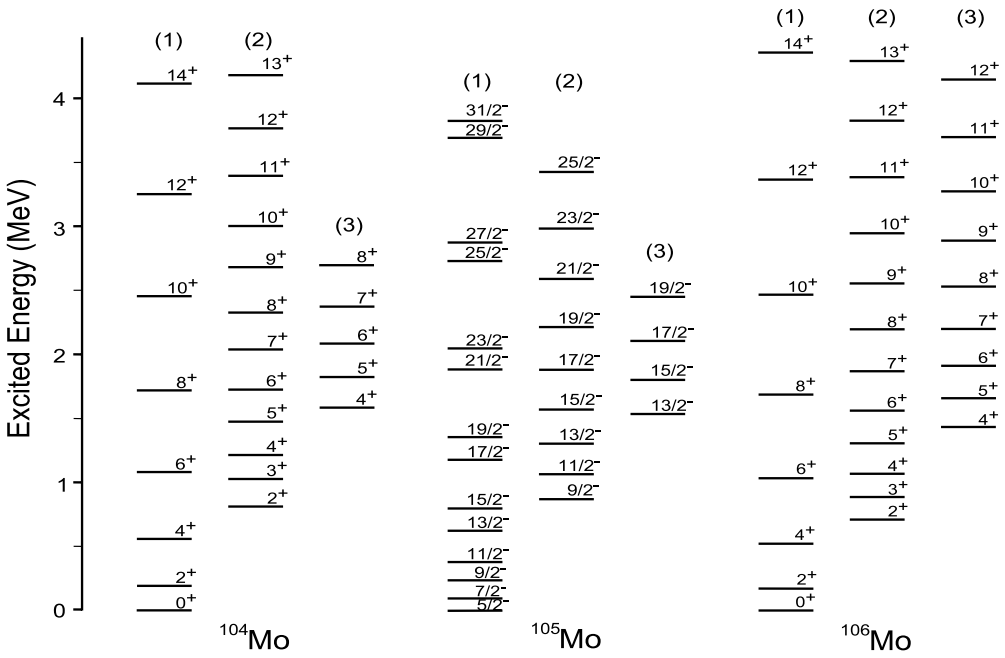

FIG. 10. Systematic comparison of the levels of the yrast bands; one- and two-phonon γ-vibrational bands in ^{104,105,106}Mo.

band (5). The possible spin of the band-head level is either 11/2 or 13/2. For similar reasons discussed above, we can excluded a single-particle configuration. However, as the band-head energy of 1534.6 keV is well below the neutron pairing gap $2\Delta_n \sim 2.1$ MeV and the proton pairing gap $2\Delta_p \sim 1.7$ MeV [4], we can rule out a three-quasiparticle configuration for it. Careful searches for the energetically favored, much higher energy $E2$ transitions from levels in band (6) to the $9/2^-$, $11/2^-$ levels of band (1) yielded no evidence for transitions to band (1). In the 94.9- to 266.3-kev and 94.9- to 572.1-keV gates the efficiency corrected ratios of γ intensities of the $13/2^- \rightarrow 9/2^-$, 1301.6- to 664.7-keV transitions are $<1/102$ and $<1/93$, respectively. The energy factor would favor the 1301.6-keV transition compared to the 664.7-kev transition by a factor of 32, giving a total retardation of over 3000 for the transitions from band (6) to (1) compared to those from band (6) to (5). Similar results were obtained for the ratio of the $15/2^-$–$11/2^-$ transitions from band (6) to bands (1) and (5). The fact that the band head is approximately twice the energy of the band head of band (5) and band (6) decays only to band (5) and not to the lower-energy states of band (1) indicates that the band (6) is a two-phonon γ-vibrational band with $K = 13/2$. The state at 1534.6 keV is then assigned as $13/2^-$. So both bands (5) and (6) are proposed to be collective γ-vibrational bands, which can be explained as the coupling of the single-particle $5/2^-[532]$ orbital for

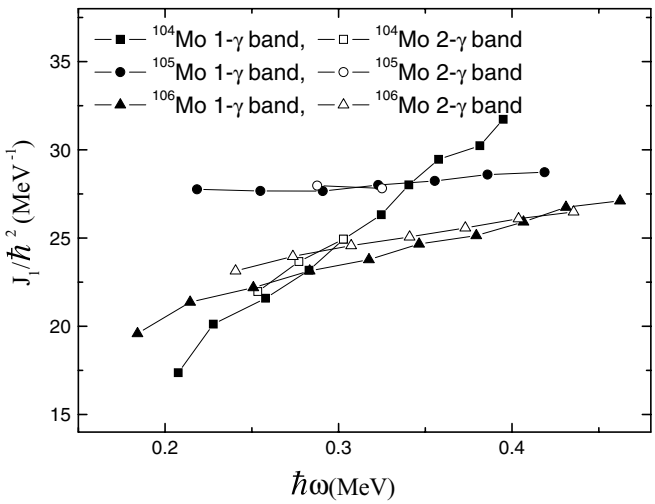

FIG. 11. Plot of moment of dynamical inertia J_1 versus rotational frequency $\hbar\omega$ for the γ-phonon vibrational bands in ^{104}Mo, ^{105}Mo and ^{106}Mo.

the ground state with one- and two-phonon γ-vibrational band cores in the neighboring even-even Mo nuclei. Figure 10 shows a systematic comparison of levels in the ground-state band, the one-phonon and the two-phonon γ-vibrational bands in ^{104}Mo [6], ^{105}Mo (the present work), and ^{106}Mo [7]. One can see that the one-phonon and two-phonon γ-vibrational bands in ^{104,105}Mo have absolute energies that are remarkably close to those in ^{106}Mo. The following have close band-head energies: 812 keV in ^{104}Mo, 871 keV in ^{105}Mo, and 710 keV in ^{106}Mo for the one-phonon γ-band and 1583 keV in ^{104}Mo, 1535 keV in ^{105}Mo, and 1818 keV in ^{106}Mo for the two-phonon γ-band. The band-head energy ratios of $E_{2\gamma}/E_{1\gamma}$ are 1.95, 1.76, and 2.56 for ^{104}Mo, ^{105}Mo, and ^{106}Mo, respectively. The characteristics of the γ band in ^{105}Mo are remarkably similar to the ones in ^{104}Mo. The similarity of the linking de-excitation transitions between the one-phonon γ bands and the ground-state bands as well as between the one-phonon and the two-phonon γ bands in ^{104,105,106}Mo give further evidence for our assignment.

The assignments are also supported by the fact that the yrast band, one-phonon and two-phonon γ-vibrational bands exhibit, as expected, similar inertia parameters. Fits of the three bands of ^{105}Mo to the first-order rotational energy formula

$$E_I = A[I(I+1) - K^2] + E_K \qquad (1)$$

yield very close values for the inertia parameters A: 16.4, 17.8, and 17.9 for the yrast band and the one-phonon and two-phonon γ-vibrational bands, respectively. Such close inertia parameter values in the yrast band and the one-phonon and two-phonon γ-vibrational bands in a nucleus are also observed in the neighboring even-even isotopes ^{104}Mo [5] and ^{106}Mo [14]: 22.5, 24.3, and 24.2 in ^{104}Mo and 25.5, 25.4, and 22.6 in ^{106}Mo, respectively.

The plots of the dynamical moment of inertia J_1 versus the rotational frequency $\hbar\omega$ for the one-phonon and two-phonon γ bands in ^{104,105,106}Mo are shown in Fig. 11. The curves have similar behavior as a function of $\hbar\omega$ variation for the one-phonon and two-phonon γ bands in each isotope, that is, the similar slopes of the plots of J_1 against the rotational frequency for the two bands in each isotope. Such a feature has been suggested as a characteristic of multiphonon vibrational bands, as discussed in Refs. [4,39]. However, the curve slopes show different behaviors, being rather flat in ^{105}Mo, of medium slope in ^{106}Mo, and of largest slope in ^{104}Mo. This may be caused by differently aligned angular momenta. A minimum alignment in ^{105}Mo could be related to a blocking effect from the $h_{11/2}$ single neutron.

IV. CONCLUSION

Rotational bands in neutron-rich ^{105}Mo, which were populated in the spontaneous fission of ^{252}Cf, have been reinvestigated. The data have much higher statistics than in our previous measurements. The yrast band built on the $5/2^-[532]$ Nilsson orbital has been confirmed and extended. Five new collective bands are established. Among them, the three positive-parity bands are proposed to be built on the $3/2^+[411]$, $1/2^+[411]$, and $5/2^+[413]$ Nilsson orbitals, respectively. The other two negative-parity bands have the expected properties of one-phonon and two-phonon γ-vibrational bands. This is the first observation of such γ-vibrational collective band structures in odd-A nuclei in this region. TRS calculation indicates that the ^{105}Mo nucleus has a medium triaxiality with $\gamma \sim -19^\circ$.

ACKNOWLEDGMENTS

The work at Tsinghua University was supported by the National Natural Science Foundation of China under grants 10575057 and 10375032 and the Special Program of Higher Education Science Foundation under grant 20030003090. The work at Vanderbilt University, Lawrence Berkeley National Laboratory, was supported, respectively, by U.S. Department of Energy under grant and contract DE-FG05-88ER40407 and DE-AC03-76SF00098.

[1] J. H. Hamilton, A. V. Ramayya, S. J. Zhu, G. M. Ter-Akopian, Yu. Ts. Oganessian, J. D. Cole, J. O. Rasmussen, and M. A. Stoyer, Prog. Part. Nucl. Phys. **35**, 635 (1995).
[2] M. A. C. Hotchkis *et al.*, Nucl. Phys. **A530**, 111 (1991).
[3] S. Zhu *et al.*, Rev. Mex. Fis. **38**, Suppl., 53 (1992).
[4] A. Guessous *et al.*, Phys. Rev. Lett. **75**, 2280 (1995).
[5] A. Guessous *et al.*, Phys. Rev. C **53**, 1191 (1996).
[6] L. M. Yang *et al.*, Chin. Phys. Lett. **18**, 24 (2001).
[7] R. Q. Xu *et al.*, Chin. Phys. Lett. **19**, 180 (2002).
[8] H. Hua, C. Y. Wu, D. Cline, A. B. Hayes, R. Teng, R. M. Clark, P. Fallon, A. Goergen, A. O. Macchiavelli, and K. Vetter, Phys. Rev. C **69**, 014317 (2004).
[9] W. Urban, T. Rzaca-Urban, J. L. Durell, W. R. Phillips, A. G. Smith, B. J. Varley, I. Ahmad, and N. Schulz, Eur. Phys. J. A **20**, 381 (2004).
[10] S. J. Zhu *et al.*, Eur. Phys. J. A **25**, Suppl. 1, 459 (2005).
[11] J. K. Hwang *et al.*, J. Phys. G **24**, L9 (1998).
[12] H. Hua, C. Y. Wu, D. Cline, A. B. Hayes, R. Teng, R. M. Clark, P. Fallon, A. O. Macchiavelli, and K. Vetter, Phys. Rev. C **65**, 064325 (2002).
[13] J. K. Hwang *et al.*, Phys. Rev. C **56**, 1344 (1997).
[14] W. Urban, T. Rzaca-Urban, J. A. Pinston, J. L. Durell, W. R. Phillips, A. G. Smith, B. J. Varley, I. Ahmad, and N. Schulz, Phys. Rev. C **72**, 027302 (2005).
[15] Q. H. Lu *et al.*, Phys. Rev. C **52**, 1348 (1995).
[16] X. L. Che *et al.*, Chin. Phys. Lett. **21**, 1904 (2004).
[17] Z. Jiang *et al.*, Chin. Phys. Lett. **20**, 350 (2003).
[18] K. Butler-Moore *et al.*, J. Phys. G: Nucl. Part. Phys. **25**, 2253 (1999).
[19] X. Q. Zhang *et al.*, Phys. Rev. C **63**, 027302 (2001).
[20] J. A. Alcántara-Núñez *et al.*, Phys. Rev. C **69**, 024317 (2004).
[21] Ts. Venkova *et al.*, Eur. Phys. J. A **6**, 405 (1999); **15**, 429 (2002).
[22] Y. X. Luo *et al.*, Phys. Rev. C **69**, 024315 (2004).
[23] Y. X. Luo *et al.*, Phys. Rev. C **70**, 044310 (2004).

[24] M. Oshima, T. Morikawa, Y. Hatsukawa, S. Ichikawa, N. Shinohara, M. Matsuo, H. Kusakari, N. Kobayashi, M. Sugawara, and T. Inamura, Phys. Rev. C **52**, 3492 (1995).
[25] K. Shizuma, H. Ahrens, J. P. Bocquet, N. Kaffrell, B. D. Kern, H. Lawin, R. A. Meyer, K. Sistemich, G. Tittel, and N. Trautmann, Z. Phys. A **315**, 65 (1984).
[26] M. Liang, H. Ohm, B. De Sutter-Pommé, and K. Sistemich, Z. Phys. A **351**, 13 (1995).
[27] G. Lhersonneau, P. Dendooven, A. Honkanen, M. Huhta, M. Oinonen, H. Penttilä, J. Äystö, J. Kurpeta, J. R. Persson, and A. Popov, Phys. Rev. C **54**, 1592 (1996).
[28] S. J. Zhu *et al*., Chin. Phys. Lett. **15**, 793 (1998).
[29] S. J. Zhu *et al*., Phys. Rev. C **59**, 1316 (1999).
[30] S. J. Zhu *et al*., Phys. Rev. C **60**, 051304(R) (1999).
[31] S. J. Zhu *et al*., Phys. Lett. **B357**, 273 (1995).
[32] D. C. Radford, Nucl. Instrum. Methods A **361**, 297 (1995).
[33] R. Bengtsson and S. Frauendorf, Nucl. Phys. **A327**, 139 (1979).
[34] S. Frauendorf, Phys. Lett. **B100**, 219 (1981).
[35] S. Frauendorf and F. R. May, Phys. Lett. **B125**, 245 (1983).
[36] S. J. Zhu *et al*., Phys. Rev. C **65**, 014307 (2002).
[37] Y. X. Luo *et al*., J. Phys. G **31**, 1303 (2005).
[38] Y. X. Luo *et al*., Phys. Rev. C **74**, 024308 (2006).
[39] X. Wu, A. Aprahamian, J. Castro-Ceron, and C. Baktash, Phys. Lett. **B316**, 235 (1993).